YF3:Eu3+ Micro−Single Crystals: Fine Morphological Tuning and Luminescence Properties

ARTICLE *in* CRYSTAL GROWTH & DESIGN · JULY 2013

Impact Factor: 4.89 · DOI: 10.1021/cg4005467

8 AUTHORS, INCLUDING:

Zhao qi
Chinese Academy of Sciences
52 PUBLICATIONS **595** CITATIONS
SEE PROFILE

Yongchao Jia
Université catholique de Louvain
55 PUBLICATIONS **756** CITATIONS
SEE PROFILE

Wei Lü
Chinese Academy of Sciences
64 PUBLICATIONS **667** CITATIONS
SEE PROFILE

Hongpeng You
Chinese Academy of Sciences
178 PUBLICATIONS **3,417** CITATIONS
SEE PROFILE

CRYSTAL GROWTH & DESIGN

Article

pubs.acs.org/crystal

YF_3:Eu^{3+} Micro-Single Crystals: Fine Morphological Tuning and Luminescence Properties

Baiqi Shao, Qi Zhao, Ning Guo, Yongchao Jia, Wenzhen lv, Mengmeng Jiao, Wei Lü, and Hongpeng You*

State Key Laboratory of Rare Earth Resource Utilization, Changchun Institute of Applied Chemistry, Chinese Academy of Sciences, Changchun 130022, and Graduate University of the Chinese Academy of Sciences, Beijing 100049, P. R. China

Supporting Information

ABSTRACT: Uniform YF_3:Eu^{3+} micro-single crystals with diamond-like, truncated octahedral, and octahedral morphologies have been synthesized by adjusting the molar ratio of $KF/Y(NO_3)_3$ and the amount of dilute HNO_3 through a facile hydrothermal route without using any morphology controlling agent. It has been found that the excess K^+ ions favor for the formation of {111} facets. The morphological evolution has been presented on the basis of a series of time-dependent experiments, from which a truncating growth mechanism has been proposed. Besides, the investigation on morphology-dependent luminescence properties reveals that the as-obtained truncated octahedral samples exhibit the strongest orange−red emission, while the intensity of diamond-like ones is the lowest.

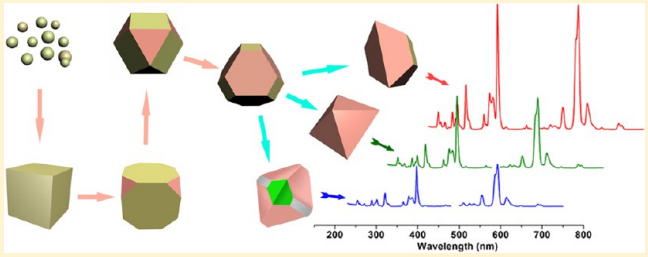

INTRODUCTION

Morphology-controlled synthesis of inorganic materials has attracted increasing interest due to their intrinsic morphology-dependent properties.[1−3] Precise control over sizes and morphologies of micro/nanocrystals enable us to manipulate their properties as desired.[4−6] Great efforts have been devoted to this issue in recent years, not only for fundamental scientific research but also for technological application.[7−11] So far, different morphologies of micro/nanocrystals have been prepared by different methods.[12−14] During the preparation process, organic surfactants or inorganic ions have often been employed as morphology controlling agents to manipulate the growth behavior of certain crystal facets and form different morphologies because their selective absorption on high-energy facets suppresses their growth rates.[15−18] However, these methods suffer from the unavoidable surface contamination due to the residual organic surfactants or ions, which affect the physical and chemical properties of the final products.[19] Therefore, a facile and environmentally friendly synthetic route free of organic surfactants still remains a challenging issue.

Because of the low vibration energies and good optical transparency over a wide wavelength range, rare earth fluorides can effectively minimize the quenching of excited state of rare earth ions during the down-conversion and upconversion luminescence processes.[20] Thus, rare earth fluorides have potential applications in optics, optoelectronics, and especially as biological labels.[21,22] Among these rare earth fluorides, YF_3 has been intensively studied due to its high effective visible or invisible light emission as a fluorescent host, and other good optical applications. Till now, YF_3 micro/nanocrystals with various morphologies have been successfully synthesized by different routes, such as high-temperature solvent,[23] reverse microemulsion,[24] template method,[25] and organic surfactant-assisted hydrothermal.[22,26] However, these methods usually need harsh reaction conditions and complicated processes, and the final products are often bound by the residual contamination. Therefore, it is a crucial issue to seek for a facile and cost-effective synthetic route free of organic surfactants.

Herein, we present a facile hydrothermal route free of organic surfactants to synthesize YF_3 microcrystals using KF as fluorine source. By tuning the amount of dilute HNO_3 and the molar ratio of $KF/Y(NO_3)_3$, diamond-like, truncated octahedral, and octahedral morphologies can be obtained. To the best of our knowledge, diamond-like morphology for YF_3 is reported for the first time, and KF is rarely used as a fluorine source. The morphological evolution and a truncating growth mechanism have been proposed on the basis of series time-dependent experiments. In addition, morphology-dependent luminescence properties have been investigated and discussed.

EXPERIMENTAL SECTION

Materials. $Y(NO_3)_3$ and $Eu(NO_3)_3$ aqueous solution was obtained by dissolving Y_2O_3 (99.99%) and Eu_2O_3 (99.99%) in dilute HNO_3 under heating with agitation. All the other chemicals are of analytical grade and used without any purification.

Preparation. In a typical procedure, 8 mL aqueous solution containing 3 mmol KF was added dropwise into 30 mL of aqueous solution containing 0.5 mmol of $Y_{0.95}Eu_{0.05}(NO_3)_3$ under magnetic stirring. When large amounts of white precipitation occurred, 0.5 mL

Received: April 12, 2013
Revised: June 4, 2013
Published: June 19, 2013

of dilute HNO_3 ($V(HNO_3)/V(H_2O)$ = 1:1) was added dropwise. After magnetic stirring for 10 min, the mixture was transferred into 50 mL Teflon-lined autoclave and heated at 180 °C for 18 h. As the autoclave cooled to ambient temperature, the products were collected and washed 3 times with water and absolute ethanol in turn, and finally dried at 60 °C in air for 12 h.

Characterizations. The phase structure and purity of the as-prepared samples were characterized by powder X-ray diffraction with a D8 Focus diffractometer (Bruker). The surface morphology and size of the as-prepared samples were inspected with a field emission scanning electron microscope equipped with an energy-dispersive spectrometer (EDS) (FE-SEM, S-4800, Hitachi, Japan). Transmission electron microscopy images were obtained using a JEOL-2010 transmission electron microscope operating at 200 kV. Photoluminescence (PL) excitation and emission spectra were recorded with a Hitachi F-4500 spectrophotometer equipped with a 150 W xenon lamp as the excitation source. All the measurements were performed at ambient temperature.

RESULTS AND DISCUSSION

Structures and Morphologies of As-Prepared YF_3 Samples. Figure 1 shows the XRD patterns of the as-prepared samples with diamond-like, octahedral, and truncated octahedral morphologies. All the peaks can be indexed to an orthorhombic phased YF_3 (JCPDS No. 74-0911) without any other impurity peaks, implying the high phase purity. In addition, the relative reflection intensity of (020) is enhanced compared with the standard diffraction pattern, indicating that the growth processes of the three occur preferentially along the [020] direction, which is further confirmed by HRTEM analysis.

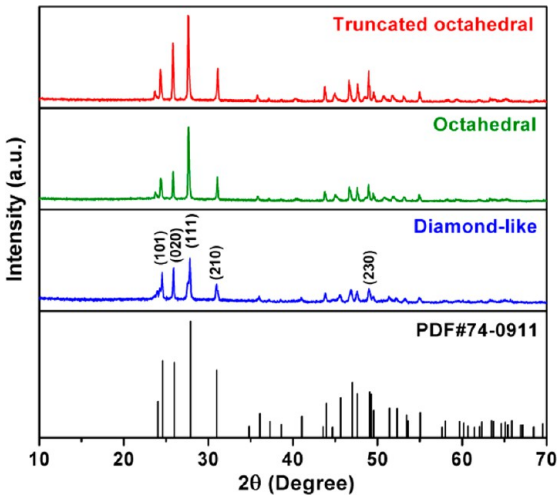

Figure 1. XRD patterns of YF_3 samples with diamond-like, octahedral, and truncated octahedral morphologies.

Figure 2 presents the morphological evolution of YF_3 samples prepared with increasing $KF/Y(NO_3)_3$ molar ratio (from up to down in columns) and the amount of dilute HNO_3 (from left to right in rows). The two reaction parameters are list in Table 1. For abbreviation, the two parameters are labeled as "$KF/Y(NO_3)_3$ molar ratio−the amount of dilute HNO_3 (mL)" in the table.

It can be seen from Figure 2, the $KF/Y(NO_3)_3$ molar ratio and the amount of dilute HNO_3 have a profound influence on the morphologies of the as-prepared products. All the samples are about 2 to 2.5 μm in hemline length with well-defined morphologies. With increasing $KF/Y(NO_3)_3$ molar ratio, the as-prepared products show a truncating tendency; while with increasing the amount of dilute HNO_3, they turn out an octahedral-formation tendency. When the $KF/Y(NO_3)_3$ molar ratio was fixed at 3 (in stoichiometric ratio), the products evolved from rough hexagonal plates to diamond-like structures as the dilute HNO_3 increased gradually. As the amount of dilute HNO_3 was fixed at 0.5 mL, the products evolved from rough octagonal plates to truncated octahedrons when $KF/Y(NO_3)_3$ molar ratio increased step by step; and these truncated octahedrons could further evolve into well-defined octahedrons with increasing amount of dilute HNO_3 at the presence of excess KF.

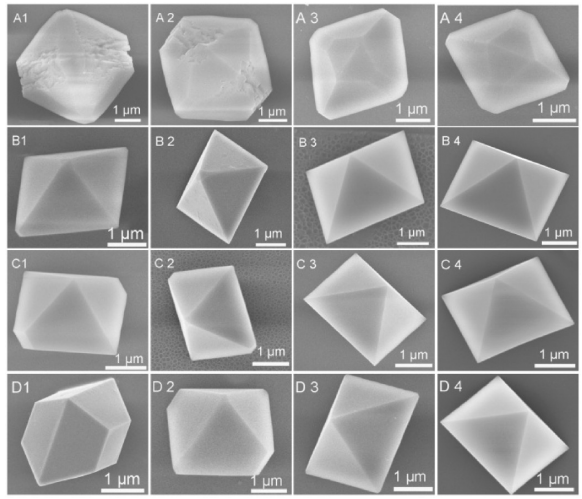

Figure 2. SEM images of YF_3:Eu^{3+} samples prepared with increasing $KF/Y(NO_3)_3$ molar ratio (from up to down in columns) and the amount of dilute HNO_3 (from left to right in rows).

Table 1. $KF/Y(NO_3)_3$ Molar Ratio−the Amount of Dilute HNO_3 (mL) for Samples

	column 1	column 2	column 3	column 4
row A	3−0.5	3−1.0	3−1.5	3−2.0
row B	4−0.5	4−1.0	4−1.5	4−2.0
row C	5−0.5	5−1.0	5−1.5	5−2.0
row D	6−0.5	6−1.0	6−1.5	6−2.0

It should be noted that the products prepared without dilute HNO_3 at the presence of excess KF are nearly monodisperse KY_3F_{10} nanoparticles with an average size of 25 nm (JCPDS No. 27-0465; Supporting Information, Figure S1). It suggests that the introduction of H^+ ions favors the formation of YF_3 at the presence of excess F^-, which may be due to the reason that H^+ ions can reduce the excess amounts of F^- ions via the reversible reaction: $H^+ + F^- \leftrightharpoons HF$, but which ion plays a dominated role in the morphological determination process needs further experimental exploration, and it will be discussed in detail later.

Careful observation of the morphological evolution of YF_3 samples gives us a clear indication that these morphologies originate from the same octahedron model. The truncated octahedron and diamond-like structure can be truncated and edge-cutted from an octahedron. The results mean that these products share mostly preferential orientations along crystal planes, which has been confirmed by XRD patterns.

More detailed structure information of diamond-like, octahedral, and truncated octahedral YF_3:Eu^{3+} samples are depicted by TEM, HRTEM images, and SAED pattern in

dx.doi.org/10.1021/cg4005467 | Cryst. Growth Des. 2013, 13, 3582−3587

Figure 3. The TEM images illustrate their morphological characteristic well, and corresponding morphology contours

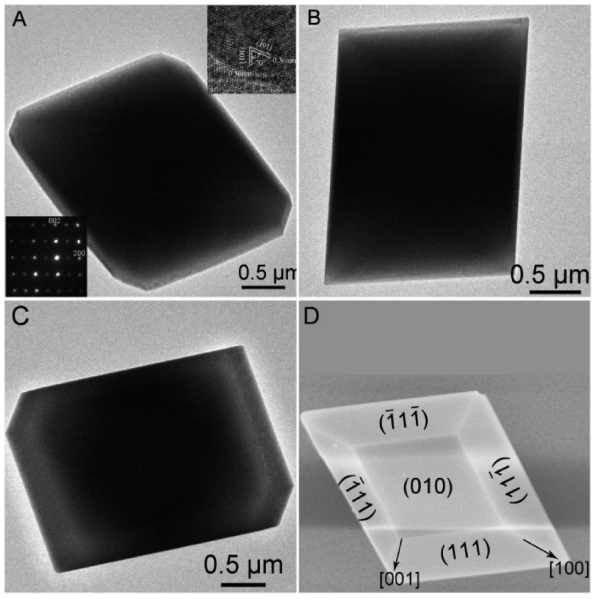

Figure 3. TEM images of an individual diamond-like (A), octahedral (B), and truncated octahedral (C) YF_3:Eu^{3+} sample and schematic illustration of the truncated octahedral sample. The inset panels in A are corresponding the HRTEM image and SAED pattern.

can be identified clearly. The distinct bright/dark contrast between the edge and center part strongly confirms their octahedral prototype, which conforms to the SEM observation. The distinct spots array in the SAED pattern (inset in Figure 3A) indicates their single crystal nature. The diffraction dots can be indexed to (002) and (200) planes of the orthorhombic phased YF_3 along the [010] zone axis. The HRTEM image (inset in Figure 3A) exhibits well-resolved 2D lattice fringes with adjacent lattice plane spacing of 0.36 nm, corresponding to (101) and (1̄01) planes. The calculated angle between [101] and [1̄01] is about 70°, which is consistent with the measured value. On the basis of the above morphological and structure evidence and the symmetries of the orthorhombic phased YF_3, we can get the conclusion that the truncated octahedral samples are enclosed by eight trapeziform {111} and two rhombic {010} facets, as illustrated in Figure 3D, which is the same with the analysis in ref 22. Following this result, we can extend the conclusion that the octahedral samples are enclosed by eight {111} facets and the diamond-like samples are enclosed by eight irregular pentagonal {111}, two rhombic {010}, four rectangular {101}, and four unidentified trapeziform facets. In this case, the crystal size perpendicular to (020) plane is larger than those of other crystal directions; and thus, the (020) relative reflection intensity will be enhanced in the corresponding XRD patterns. This analysis is consistent with the observation in the corresponding XRD patterns, especially for the truncated octahedral sample.

To determine which ion mainly does work in the morphological determination process, we have designed a series of contrast experiments. When KF was substituted by HF, the as-obtained products are all chain-like structures (Figure 4A–C) assembled by ellipsoid nanoparticles with increasing amount of HF. The ellipsoid nanoparticles are about 250 nm long and 80 nm in diameter at the middle part. To

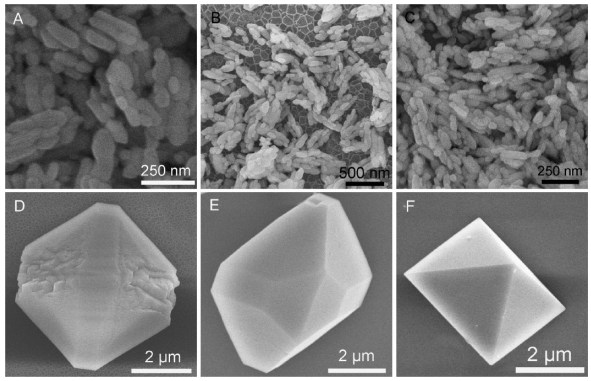

Figure 4. SEM images of YF_3:Eu^{3+} samples prepared with (A) 1.5, (B) 2, and (C) 3 mmol HF; and (D) 1.5, (E) 2, and (F) 3 mmol KNO_3 when HF was fixed at 1.5 mmol. All the samples were prepared at the presence of 0.5 mL of dilute HNO_3.

eliminate the effect of NO_3^- ions on the morphological determination process, we replaced the dilute HNO_3 with dilute HCl, while keeping the amount of H^+ ions unchanged. The obtained products still are chain-like structures (Supporting Information, Figure S2) as described above, implying that F^- or NO_3^- ions have little influence on the morphologies of final products. However, when the stoichiometric amount of HF and increasing amount of KNO_3 were added, the as-obtained products evolved from well-defined octagonal microplates (Figure 4D) to diamond-like structure (Figure 4E) and finally to octahedron (Figure 4F), which are exactly the same with corresponding samples (Figure 3A) prepared with KF. The as-obtained samples are about 3 to 4 μm in hemline length, slightly bigger than those shown in Figure 3. These results make a clear indication that K^+ ions play a dominated role in the morphological determination process. When the amounts of K^+ ions are relatively low without excess of F^- ions, the as-obtained diamond-like products (Figure 2, sample A4) are enclosed mainly by {111} facets; while at the presence of excess K^+ ions and a spot of F^- ions (most excess F^- ions are stabilized in the form of HF at the presence of excess H^+), the as-obtained octahedral products (Figure 2, samples B4, C4, and D4) are enclosed all by {111} facets. However, when the amount of F^- is a little high at the presence of excess of K^+ ions, the as-obtained truncated octahedral products are enclosed by {111} and {010} facets. It can be concluded from the results that precise control on the amounts of K^+ and F^- ions can effectively tune the final morphologies of the products, and the excess K^+ ions favor the formation of {111} facets. Besides, the KNO_3-varying experiments and the time-dependent experiments can also suggests that the excess K^+ ions benefit a more smooth surface and make the architectures more regular, and relative insufficient K^+ ions may facilitate the formation of {100}, {101}, and some unidentified facets in diamond-like structures.

Possible Growth Mechanism. In order to understand the growth mechanism of YF_3:Eu^{3+} microcrystals, a series of time-dependent experiments have been conducted, taking truncated octahedral YF_3 microcrystals for example. The XRD patterns and SEM observations of intermediate products are employed to track the evolutions of crystalline phase and morphologies.

The initial precipitation is nearly monodisperse nanoparticles with rough surface and about 100 nm in diameter as shown in Figure S3 (Supporting Information). TEM image implies that these nanoparticles are assembled by some smaller particles.

dx.doi.org/10.1021/cg4005467 | Cryst. Growth Des. 2013, 13, 3582–3587

However, according to XRD analysis, the products cannot be indexed to a binary or ternary fluoride; the corresponding EDX spectrum confirms the existence of F, Y, and K elements. The existence of Si originates from the sample supporting substrate. After hydrothermal reaction for 1 h, the as-obtained products (Figure 5A) are monodisperse nanoparticles with an average

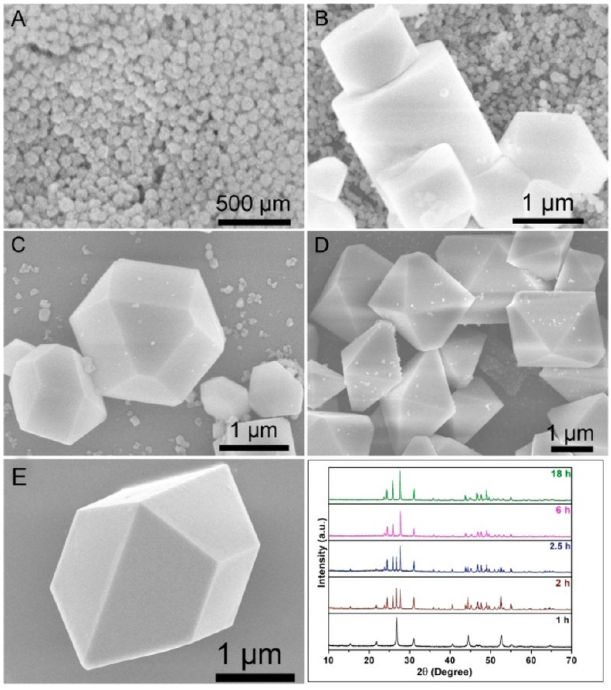

Figure 5. SEM images of YF_3 samples prepared for (A) 1, (B) 2 , (C) 2.5, (D) 6, and (E) 18 h and corresponding XRD patterns.

diameter of 90 nm, and the corresponding XRD pattern shows that these products are mainly tetragonal phased KY_3F_{10} (JCPDS No. 27-0465) with some weak peaks of hexagonal phased KYF_4. Prolonging the reaction time to 2 h, cubes and truncated cubes (Figure 5B) appeared, and these structures further evolved to cuboctahedrons (Figure 5C) within half-hour; meanwhile, the above-mentioned ternary fluoride nanoparticles were gradually consumed. The XRD patterns (2 and 2.5 h) confirm the coexistence of YF_3 and the mentioned ternary fluoride. The concomitant emergence of YF_3 diffraction peaks when the polyhedrons appeared indicates that these polyhedrons are YF_3 to a great extent. Further prolonging the reaction time to 6 h, the as-obtained products (Figure 5D) are truncated octahedrons with a spot of nanoparticles remained. Finally, the ternary fluoride nanoparticles disappeared, and the truncating tendency of truncated octahedrons (Figure 5E) is more distinct and well-defined after reaction time for 18 h. The enhancement of (020) peak in the corresponding XRD pattern agrees well with the SEM observation.

On the basis of time-dependent morphological evolution, we proposed a truncating growth mechanism, as illustrated in Figure 6. At early reaction stage, the amorphous precipitation rapidly crystallized into ternary fluorides (KY_3F_{10} and KYF_4) under hydrothermal treatment. Then the newly formed ternary fluorides transformed into more stable YF_3 phase by reacting with H^+ ions in the turbulent and acidic hydrothermal environment. The equations can be described as

$$KY_3F_{10} + H^+ = K^+ + HF + 3YF_3 \quad (1)$$

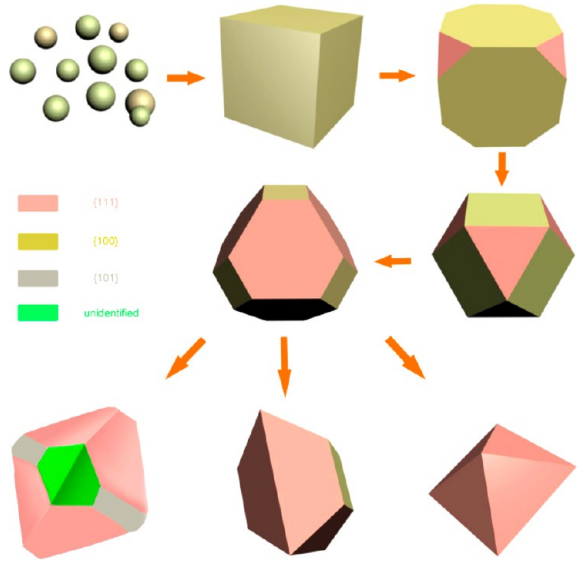

Figure 6. Schematic illustration of the truncating growth mechanism of YF_3 samples with diamond-like, truncated octahedral, and octahedral morphologies.

$$KYF_4 + H^+ = K^+ + HF + YF_3 \quad (2)$$

Meanwhile, the newly released and primary K^+ ions preferentially adsorbed on the {100} facets of the newly formed YF_3 particles. As a result, the {100} facets are stabilized and lead to the formation of YF_3 cubes. As the transformation process continues, the amounts of K^+ ions increased gradually and became the dominating ions in the reaction system. The results lead to the fact that their preferential adsorption behavior changes from {100} facets to {111} facets, and thus, the products gradually evolved to truncated cubes, cuboctahedrons, and finally to diamond-like, truncated octahedral, and octahedral morphologies, which are mainly or all enclosed by {111} facets due to the different amounts of K^+ ions.

In conclusion, K^+ ions play a dominant role in the morphological determination process in our synthesis, and H^+ ions perform 2-fold functions: one is that they facilitate the transformation of ternary fluorides to YF_3; the other is that they decrease the amounts of free F^- ions in the form of HF, which ensure the full play of K^+ ions in the morphological determination process. These results may provide some guidance in the selective synthesis of rare earth fluoride via the facile inorganic ions assisted hydrothermal strategy.

Luminescence Properties. Figure 7 shows the excitation and emission spectra of the as-prepared YF_3: Eu^{3+} samples with diamond-like, octahedral, and truncated octahedral morphologies. It can be seen that all the three samples share the identical spectral pattern with distinct difference in intensity. The excitation spectra (monitored at 592 nm) consists of several intense and sharp lines corresponding to the direct excitation of the ground state into excited states of 4f-electrons of the Eu^{3+} ions, which are practically identical to the characteristic absorption bands for the f−f intraconfiguration transitions of the Eu^{3+} ions. The dominant absorption peak is centered at 397 nm, which can be assigned to the $^7F_{0,1}-^5L_6$ transition of the Eu^{3+} ions, and the other relative weaker lines can be assigned to $^7F_{0,1}-^5D_{2,3,4}$ (466, 417, and 320 nm, respectively), $^7F_{0,1}-^5G_J$ (centered at 378 nm), and $^7F_{0,1}-^5F_1$ (362 nm). In general, Eu^{3+}-doped oxide phosphors usually exhibit a wide excitation

dx.doi.org/10.1021/cg4005467 | Cryst. Growth Des. 2013, 13, 3582−3587

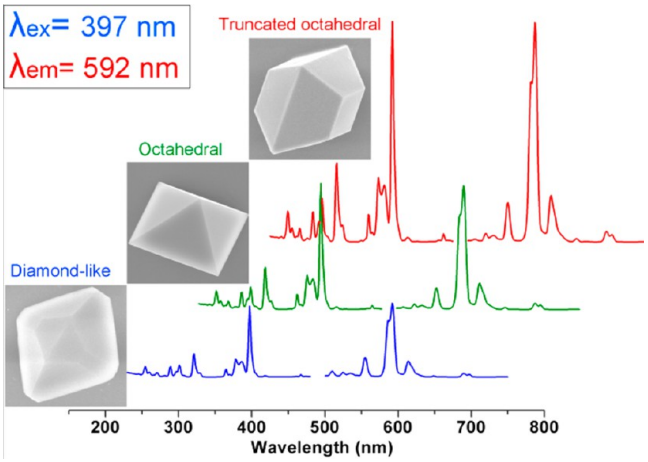

Figure 7. Excitation and emission spectra of YF_3:Eu^{3+} samples with diamond-like, octahedral, and truncated octahedral morphologies.

band in the UV region (200−300 nm) due to the charge-transfer (CT) transition from the filled 2p-shell of the ligands to the partially filled 4f-shell of Eu^{3+} ions. However, no notable intense band can be observed in the excitation spectra. This is because F^- ions exhibit higher electronegativity, and thus, the CT transition process needs much more energy compared with Eu^{3+}-doped oxide phosphors. As a result, the CT band would locate into the vacuum ultraviolet region.

Upon UV excitation at 397 nm, the emission spectra show typical orange−red emission of the Eu^{3+} ions. The emission spectra consist of a group characteristic lines corresponding to the $^5D_2$−$^7F_3$ (510 nm), $^5D_1$−$^7F_{0,2}$ (524 and 555 nm), and $^5D_0$−^7F_J (J = 1−4; 592, 614, 650, and 690 nm) transitions in the Eu^{3+} ions, respectively. It is well-known that the emission intensity ratio of the $^5D_0$−$^7F_1$ to $^5D_0$−$^7F_2$ reflects the symmetry of the crystal sites where Eu^{3+} ions occupy, and therefore, Eu^{3+} ions are often used as probes to detect the environment of the lanthanide ions. Generally, in a site with inversion symmetry, the $^5D_0$−$^7F_1$ magnetic dipole transition is dominant, while the $^5D_0$−$^7F_2$ forced electric dipole transition will be the strongest one if Eu^{3+} ions occupy the sites without inversion symmetry, which is hypersensitive to relatively small change in the chemical surrounding of Eu^{3+} ions.[27] In YF_3: Eu^{3+} crystal structure, Eu^{3+} ions occupy the site of Y^{3+} with C_s site symmetry, and the noncentrosymmetry is supposed to favor the higher intensity of the $^5D_0$−$^7F_2$ forced electric dipole transition. However, the $^5D_0$−$^7F_1$ magnetic dipole transition (592 nm) takes the dominating place, this is because the high ionicity of the Eu−F bonds allows only a little admixture of opposite parity states to the Eu^{3+} f-state, and then the $^5D_0$−$^7F_2$ forced electric dipole transition is far less favorable.[28]

For luminescence intensity, comparing all the three samples as shown in Figure 7, the truncated octahedral samples exhibit the strongest emission, the octahedral samples take the second place, and the diamond-like samples are relatively weaker. The dramatic difference can be attributed to the combined effects of crystallinity and the amounts of defects. Usually, lower crystallinity means poor order in structure and more defects, which should be responsible for weak luminescence. The variation tendency of luminescence intensity of the three samples is consistent with the degree of their crystallinity (Figure 1). Besides, the diamond-like samples tend to be plate-like morphology, which possess longer and thinner edges and more apexes compared with the other two samples. Generally, there will be more defects at these special junctions of facets than other geometric locations. A careful observation showed that there are some casting defects at the arrises of the diamond-like samples (Figure 4A), suggesting the existence of crystal defects directly. During the luminescence process, defect is an important pathway for nonradiative relaxation, which can form quenching center and lead to nonradiative recombination and luminescence quenching. As a result, the diamond-like samples exhibit relatively weak luminescence compared with the octahedral and truncated octahedral samples.

The decay kinetics behavior of the three samples have also been investigated, the corresponding decay curves for the luminescence of the Eu^{3+} ions (λ_{em} = 592 nm, $^5D_0$−$^7F_1$) are shown in Figure 8. All the curves can be fitted into a single

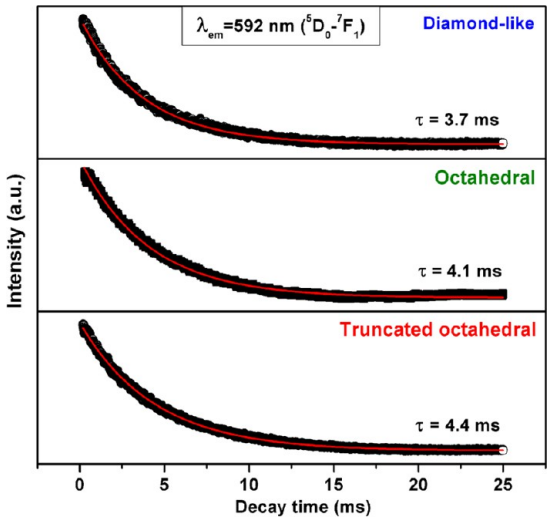

Figure 8. Decay curves of the $^5D_0$−$^7F_1$ emission of Eu^{3+} in YF_3:Eu^{3+} samples with diamond-like, octahedral, and truncated octahedral morphologies.

exponential function as $I(t) = I_0 \exp(-t/\tau)$, and the lifetimes are determined to be 3.7, 4.1, and 4.4 ms for diamond-like, octahedral, and truncated octahedral sample, respectively. The lifetime sequence is consistent with the variation tendency of the luminescence intensity of the three samples, which is attributed to the increase of nonradiative transition rate caused by surface defects.[29] As discussed above, the amount of defects in diamond-like sample is larger than that of the two other ones, and thus the lifetime is shorter.

CONCLUSIONS

In summary, uniform YF_3:Eu^{3+} micro-single crystals with diamond-like, truncated octahedral, and octahedral morphologies have been synthesized using KF as fluorine source by a facile hydrothermal route without using any morphology controlling agent on the basis of the fact that the excess K^+ ions favor for the formation of {111} facets. By tuning the amount of dilute HNO_3 and the molar ratio of KF/$Y(NO_3)_3$, regular morphological evolution has been observed. The morphological evolution and a truncating growth mechanism have been proposed on the basis of a series of time-dependent experiments. Morphology-dependent luminescence properties investigation shows that the emission intensity increases dramatically from the diamond-like sample to the octahedral one and finally to the truncated octahedral one, which may arise

dx.doi.org/10.1021/cg4005467 | Cryst. Growth Des. 2013, 13, 3582−3587

from the difference in the crystallinity and the amounts of surface defects.

■ ASSOCIATED CONTENT

Supporting Information

SEM, XRD, XED, and EDX images. This material is available free of charge via the Internet at http://pubs.acs.org.

■ AUTHOR INFORMATION

Corresponding Author

*(H.Y.) E-mail: hpyou@ciac.jl.cn.

Notes

The authors declare no competing financial interest.

■ ACKNOWLEDGMENTS

This work is financially supported by the National Natural Foundation of China (Grant No. 21271167) and the Fund for Creative Research Groups (Grant No. 21221061).

■ REFERENCES

(1) Ahmadi, T. S.; Wang, Z. L.; Green, T. C.; Henglein, A.; El-Sayed, M. A. *Science* **1996**, *272*, 1924.
(2) Cushing, B. L.; Kolesnichenko, V. L.; O'Connor, C. J. *Chem. Rev.* **2004**, *104*, 3893.
(3) Tao, A. R.; Habas, S.; Yang, P. *Small* **2008**, *4*, 310.
(4) Sun, S.; Murray, C. B.; Weller, D.; Folks, L.; Moser, A. *Science* **2000**, *287*, 1989.
(5) Sun, Y.; Xia, Y. *Science* **2002**, *298*, 2176.
(6) Liu, K.; You, H.; Jia, G.; Zheng, Y.; Song, Y.; Yang, M.; Huang, Y.; Zhang, H. *Cryst. Growth Des.* **2009**, *9*, 3519.
(7) Peng, K.-Q.; Wang, X.; Li, L.; Hu, Y.; Lee, S.-T. *Nano Today* **2013**, *8*, 75.
(8) Chen, S.; Bi, J.; Zhao, Y.; Yang, L.; Zhang, C.; Ma, Y.; Wu, Q.; Wang, X.; Hu, Z. *Adv. Mater.* **2012**, *24*, 5593.
(9) Wang, J.; Gao, W. *ACS Nano* **2012**, *6*, 5745.
(10) Sassoye, C.; Patriarche, G.; Mortier, M. *Opt. Mater.* **2009**, *31*, 1177.
(11) Lei, F.; Yan, B.; Chen, H.-H.; Zhang, Q.; Zhao, J.-T. *Cryst. Growth Des.* **2009**, *9*, 3730.
(12) Wang, C.; Daimon, H.; Onodera, T.; Koda, T.; Sun, S. *Angew. Chem., Int. Ed.* **2008**, *47*, 3588.
(13) Hu, L.; Peng, Q.; Li, Y. *J. Am. Chem. Soc.* **2008**, *130*, 16136.
(14) Wang, Y.-H. A.; Zhang, X.; Bao, N.; Lin, B.; Gupta, A. *J. Am. Chem. Soc.* **2011**, *133*, 11072.
(15) Bu, W.; Chen, Z.; Chen, F.; Shi, J. *J. Phys. Chem. C* **2009**, *113*, 12176.
(16) Chen, C.; Hu, R.; Mai, K.; Ren, Z.; Wang, H.; Qian, G.; Wang, Z. *Cryst. Growth Des.* **2011**, *11*, 5221.
(17) Du, Y.-P.; Sun, X.; Zhang, Y.-W.; Yan, Z.-G.; Sun, L.-D.; Yan, C.-H. *Cryst. Growth Des.* **2009**, *9*, 2013.
(18) Wu, M.; Lin, G.; Chen, D.; Wang, G.; He, D.; Feng, S.; Xu, R. *Chem. Mater.* **2002**, *14*, 1974.
(19) Yang, C.-C.; Yu, Y.-H.; van der Linden, B.; Wu, J. C. S.; Mul, G. *J. Am. Chem. Soc.* **2010**, *132*, 8398.
(20) Yan, R. X.; Li, Y. D. *Adv. Funct. Mater.* **2005**, *15*, 763.
(21) Corstjens, P. L. A. M.; Zuiderwijk, M.; Nilsson, M.; Feindt, H.; Sam Niedbala, R.; Tanke, H. J. *Anal. Biochem.* **2003**, *312*, 191.
(22) Tao, F.; Wang, Z.; Yao, L.; Cai, W.; Li, X. *Cryst. Growth Des.* **2007**, *7*, 854.
(23) Wang, S.; Xu, H.; Chen, X.; Zhong, S.; Jiang, J.; Huang, Y.; Wang, S.; Xu, R. *J. Cryst. Growth* **2008**, *310*, 4697.
(24) Lemyre, J.-L.; Ritcey, A. M. *Chem. Mater.* **2005**, *17*, 3040.
(25) Shchukin, D. G.; Sukhorukov, G. B. *Langmuir* **2003**, *19*, 4427.
(26) Zhang, M.; Fan, H.; Xi, B.; Wang, X.; Dong, C.; Qian, Y. *J. Phys. Chem. C* **2007**, *111*, 6652.
(27) Zheng, Y.; You, H.; Jia, G.; Liu, K.; Song, Y.; Yang, M.; Zhang, H. *Cryst. Growth Des.* **2009**, *9*, 5101.
(28) Lezhnina, M. M.; Jüstel, T.; Kätker, H.; Wiechert, D. U.; Kynast, U. H. *Adv. Funct. Mater.* **2006**, *16*, 935.
(29) Song, Y.; You, H.; Huang, Y.; Yang, M.; Zheng, Y.; Zhang, L.; Guo, N. *Inorg. Chem.* **2010**, *49*, 11499.